Chapter in **Advancing Astrophysics with the SKA – II**

Beyond ΛCDM with the SKA Observatory – I Probing Gravity on Cosmological Scales

S. Camera,[1,2,3,4] C. Addis,[5] S.L. Guedezounme,[4] F. Montano,[1,2] T. Montandon,[6] M. Novara,[1,2] S.J. Rossiter,[1,2] J. Asorey,[7] S. Castello,[8] C. Clarkson,[5,4] J. Fonseca,[9,10,4] N. Frusciante,[11,12] C. Gomes,[13,14] N. Grimm,[15,8] A. Nasirudin,[16] L.G.T. Oliveira,[9,10] F. Pace,[1,2,3] Z. Sakr,[17,18,19] M. Berti,[8] C. Bonvin,[8] P. Bull,[16,4] E. Di Dio,[8] C. Cress,[20] C. Heneka,[21] H.-R. Klöckner,[22] R. Maartens,[4] C.J.A.P. Martins,[9,23] D. Parkinson[24] and C.S. Saraf[24]

[1]*Dipartimento di Fisica, Università degli Studi di Torino, 10125 Torino, Italy*
[2]*INFN – Istituto Nazionale di Fisica Nucleare, Sezione di Torino, 10125 Torino, Italy*
[3]*INAF – Istituto Nazionale di Astrofisica, Osservatorio Astrofisico di Torino, 10025 Pino Torinese, Italy*
[4]*Department of Physics & Astronomy, University of the Western Cape, Cape Town 7535, South Africa*
[5]*Astronomy Unit, Department of Physics & Astronomy, Queen Mary University of London, E1 4NS, U.K.*
[6]*Laboratoire Univers et Particules, CNRS & Université de Montpellier, 34095 Montpellier, France*
[7]*Departamento de Física Teórica, Centro de Astropartículas y Física de Altas Energías (CAPA), Universidad de Zaragoza, 50009 Zaragoza, Spain*
[8]*Département de Physique Théorique and Center for Astroparticle Physics, Université de Genève, CH-1211 Geneva 4, Switzerland*
[9]*Instituto de Astrofísica e Ciências do Espaço, Universidade do Porto CAUP, 4150-762 Porto, Portugal*
[10]*Faculdade de Ciências, Universidade do Porto, 4169-007 Porto, Portugal*
[11]*Dipartimento di Fisica "E. Pancini", Università degli Studi di Napoli "Federico II", 80126 Napoli, Italy*
[12]*INFN – Istituto Nazionale di Fisica Nucleare, Sezione di Napoli, 80126 Napoli, Italy*
[13]*Centro de Física das Universidades do Minho e do Porto, Faculdade de Ciências, Universidade do Porto, 4169-007 Porto, Portugal*
[14]*OKEANOS, Universidade dos Açores, 9900-140 Horta, Portugal*
[15]*Institute of Cosmology & Gravitation, University of Portsmouth, Portsmouth PO1 3FX, U.K.*
[16]*Jodrell Bank Centre for Astrophysics, The University of Manchester, Manchester M13 9PL, U.K.*
[17]*Instituto de Física Teórica UAM-CSIC, Universidad Autónoma de Madrid, 28049 Madrid, Spain*
[18]*Institut de Recherche en Astrophysique et Planétologie (IRAP), Université de Toulouse, CNRS, UPS, CNES, 31400 Toulouse, France*
[19]*Faculty of Sciences, Université Saint-Joseph de Beyrouth, Beirut BP-11514, Lebanon*
[20]*Department of Mathematical Sciences, University of South Africa, Roodepoort 1709, South Africa*
[21]*Institut für Theoretische Physik, Universität Heidelberg, 69120 Heidelberg, Germany*
[22]*Max-Planck-Institut für Radioastronomie, 53121 Bonn, Germany*
[23]*Centro de Astrofísica da Universidade do Porto, 4150-762 Porto, Portugal*
[24]*Korea Astronomy and Space Science Institute, Daejeon 34055, Republic of Korea*

E-mail: stefano.camera@unito.it

General relativity (GR) is currently the best description of the gravitational interaction at our disposal and is one of the foundations of the concordance cosmological model. For as much as we know that GR is not the final theory of gravitation—we still lack an understanding of its fundamental, quantum nature—it has demonstrated a remarkable success in describing observed phenomena and predicting effects that have later been confirmed by laboratory experiments or astronomical observations. Since gravity is extremely weak compared to the other three fundamental interactions, it has so far been tested with exquisite precision only in the strong-field regime. On the immense scales of the cosmos, on the other hand, the gravitational field is extremely weak and spacetime curvature is almost negligible. But crucially, it is on these scales that we see hints at the need for exotic components, such as dark matter and dark energy. The question of whether they really exist or their presence is but an artifact of the incompleteness of our understanding of gravity on cosmological scales then naturally arises. It is therefore paramount to test the validity of GR on these scales, either to further confirm its robustness or to detect deviations that could lead us to the formulation of a more general and conclusive theory of gravitation. To this purpose, the SKA Observatory is especially suited, thanks both to the enormous volumes it will probe, and to the variety and complementarity of cosmological observables that its surveys will make available to us.

Contents

1 Introduction

Over the past decades, the so-called concordance cosmological model, ΛCDM, has provided us with a remarkably successful description of the Universe on large scales. It rests on two pillars: general relativity (GR), to describe the gravitational interaction, and the Standard Model of Particle Physics, accounting for the content of the Universe as well as for the interplay between it and the other three known fundamental interactions. In addition to such pillars, it is then necessary to hypothesise the presence of a yet-unknown cold dark matter (CDM) component, and a cosmological constant (Λ) as the driver of the observed late-time accelerated expansion of the cosmos. Among the remarkable successes of the ΛCDM model are the reproduction of the observed expansion history and the cosmic microwave background (CMB) anisotropies, and of the statistical properties of the large-scale distribution of galaxies, with impressive precision (see e.g. Planck Collaboration: Aghanim et al., 2020; Alam et al., 2021). However, ΛCDM faces a number of conceptual and observational challenges that motivate the exploration of alternatives. The focus of this chapter is thus particularly on testing the first pillar, i.e. the validity of GR as the correct theory of gravity on cosmological scales.

From a theoretical standpoint, the cosmological constant problem remains one of the deepest puzzles in modern physics. The observed value of Λ, corresponding to an energy density of roughly 10^{-120} in Planck units, is inexplicably small compared to the natural scales predicted by quantum field theory (Weinberg, 1989; Padmanabhan, 2003). This extreme fine-tuning, together with the so-called coincidence problem—why are the density of matter and that associated to Λ comparable today?—has led to a long-standing search for a dynamical explanation of cosmic acceleration. Cosmologists have tried to model the accelerated expansion with two alternative approaches. The first assumes that GR is valid on all (macroscopic) scales and then introduces a significant fraction of dark energy, intended as an evolving component whose present-day value is almost indistinguishable from a

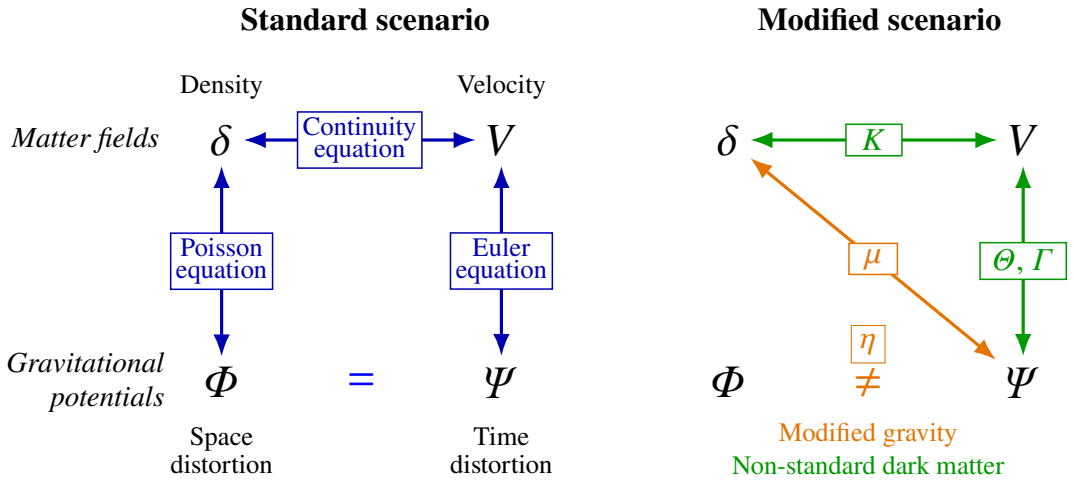

Figure 1: Fundamental relations between the matter fields and the gravitational potentials in the standard cosmological model (left) and with generic deviations due to gravity modifications and non-standard dark matter properties (right). The deviations on the right panel are generic free functions of redshift and scale. (Reproduced from Castello 2025.)

simple cosmological constant (see Navas et al., 2024, and references therein, for a comprehensive review). Alternatively, the acceleration can be modelled as an emergent effect from modifications of gravity on cosmological scales (see e.g. Clifton et al., 2012).

To get some intuition, let us consider Fig. 1. Cosmological observables essentially probe the four fields presented there and their interrelations. On cosmological scales, we see (left panel) how GR predicts a precise relation between the content of the Universe and the distortions its presence causes on space—namely, the relativistic Poisson equation—as well as how space and time distortions are related. The continuity and Euler equations instead arise from the conservation of the stress-energy tensor, with cosmic acceleration being due to the cosmological constant or a dynamical dark energy component. Evidence of any modification to this standard scenario (right panel) will guide us to its source, and the advent of next-generation surveys offers unprecedented opportunities to test these scenarios (for a review on the topic, see also Ishak, 2019).

In this context, the SKA Observatory (SKAO) will play a transformative role in probing the nature of dark energy and gravity. With its large sky coverage, wide redshift range, and exquisite sensitivity, the SKAO will provide us with a diverse and complementary set of cosmological observables, which could also be analysed jointly with more traditional cosmological observables at microwave and optical/near-infrared wavelengths. By measuring the expansion rate and the angular diameter distance through baryon acoustic oscillations and redshift-space distortions (RSDs), and the growth rate of structures, which depends directly on the underlying theory of gravity, the SKAO can tightly constrain deviations from GR. Moreover, the various cosmological probes available to us thanks to the SKAO will allow for powerful, model-independent consistency tests (Camera et al., 2015; Baker et al., 2021).

The synergistic potential of the SKAO with traditional optical/near-infrared surveys for cosmology

will further enhance its ability to trace both geometry and the growth of cosmic structures, contributing to lifting degeneracies and uncovering possible scale-dependent deviations from GR. The coming decades will hence be pivotal in determining whether cosmic acceleration arises from an evolving dark energy component or from a breakdown of GR on cosmological scales. Accordingly, the present chapter is structured to reflect these two possibilities. After having introduced the main observables in Section 2, Section 3 will outline how cosmological surveys with the SKAO will be able to test the validity of GR on cosmological scales. Conversely, Section 4 will focus on the capabilities of the SKAO in detecting signatures of modified gravity. Section 5 will present additional probes to test gravity with the SKAO. Future perspectives, also in the view of possible upgrades of the instrument and technological advancements, will be discussed in Section 6. Finally, conclusions will be drawn in Section 7.

2 Target observables and summary statistics

In the study of the cosmic large-scale structure (LSS), two cosmological probes have been identified by the scientific community as particularly promising: galaxy clustering and cosmic shear. The former scrutinises the statistical properties of fluctuations in the observed number counts of galaxies, whereas the latter extracts information from the distorted shapes of distant galaxy images, in the regime of weak gravitational lensing deflections. At the state of the art, they are, respectively, the primary targets of spectroscopic surveys performed e.g. by the Dark Energy Spectroscopic Instrument (DESI, DESI Collaboration: Abareshi et al., 2022; DESI Collaboration: Abdul-Karim et al., 2025) or imaging surveys like the Legacy Survey of Space and Time (LSST, Ivezić et al., 2019; The LSST Dark Energy Science Collaboration: Mandelbaum et al., 2018) at the Vera C. Rubin Observatory. Each observable is a powerful source of information in itself, but it is well-known that their combination opens up transformational possibilities, such as detecting deviations from GR on cosmological scales (Hu and Jain, 2004; Bernstein and Jain, 2004). It is precisely for this reason that the European Space Agency's flagship, the *Euclid* satellite, was designed in the first place (Euclid Collaboration: Mellier et al., 2025).

In this context, the field of radio cosmology will be revolutionised by the SKAO (Maartens et al., 2015; SKA Cosmology SWG: Bacon et al., 2020), thanks to the new observables that it will make available and their cross-correlations with clustering and shear measured by traditional means. Among such new observables, neutral hydrogen (HI) intensity mapping stands out. It is a revolutionary new way of mapping the LSS by measuring the aggregate line emission from all of the gas and galaxies within a relatively large volume element, thus obtaining high-fidelity representations of the underlying matter distribution (Bharadwaj et al., 2001; Loeb and Wyithe, 2008). Currently, surveys carried out at so-called precursor and pathfinder facilities (Norris et al., 2011; Santos et al., 2016; Shimwell et al., 2017) are already demonstrating the enormous potential of future SKAO observational campaigns for cosmology.

Finally, even gravitational wave (GW) observations can be exploited to probe the LSS, e.g. with LIGO, Virgo, and Kagra (Abac et al., 2025b), the Einstein Telescope (ET, Abac et al., 2025a), or the Laser Interferometer Space Antenna (LISA, Auclair et al., 2023). We thus expect plenty of varied data sets to be available in the upcoming years to investigate the cosmic LSS.

We shall now briefly outline the two main cosmological fields under consideration: the density contrast of a tracer t of the underlying LSS, Δ_t, and the weak gravitational lensing effect of cosmic shear, γ. For more details on clustering and lensing in an SKAO context, we refer the reader to the following other chapters of the present science book: Nasirudin et al. (2026, for HI-line galaxies), Asorey&Hale et al. (2026, for radio-continuum galaxies), Wolz et al. (2026, for HI intensity mapping), Harrison et al. (2026b, for radio weak lensing), and Harrison et al. (2026a, for cross-correlations among the aforementioned probes).

Galaxy clustering and HI intensity mapping

Fluctuations in galaxy number density trace perturbations in the underlying matter density via multiple effects. In a fully general-relativistic treatment, various sub-dominant contributions arise as a consequence of the propagation of photons in an inhomogeneous universe and we consider these below. In the linear regime, where cosmological perturbations are small, the number density contrast can be schematically written as the sum of various contributions (see Yoo et al., 2009; Bonvin and Durrer, 2011; Challinor and Lewis, 2011; Jeong et al., 2012),

$$\Delta_t = \Delta_t^{(\mathrm{den})} + \Delta_t^{(\mathrm{vel})} + \Delta_t^{(\mathrm{len})} + \Delta_t^{(\mathrm{rel})} \,, \tag{1}$$

where t labels any given galaxy population tracing the underlying LSS. The first term captures the effect of matter density perturbations, given by the galaxy bias b_t times the matter density contrast δ. The second one includes contributions due to peculiar velocities, which perturb the observed redshift. The dominant of these velocity contributions is the well-known RSD effect (Kaiser, 1987; Zaroubi and Hoffman, 1993), $\Delta^{(\mathrm{RSD})} \subset \Delta_t^{(\mathrm{vel})}$. However, $\Delta_t^{(\mathrm{vel})}$ also contains a relativistic Doppler term that is typically not considered in RSD analyses. The third term describes the increase/depletion of galaxy number counts caused by lensing magnification. Increase is due to more sources falling within the detection threshold thanks to their flux being amplified by lensing, whilst depletion may happen because of the stretch of the distorted solid angle, which may make sources at the edge of an observed patch fall out of the area. Finally, the last term collects all other contributions, collectively referred to as 'relativistic'. Among such terms are an integrated Sachs-Wolfe effect, time delay, and gravitational redshift.

Typically, only the dominant terms $\Delta_t^{(\mathrm{den})} = b_t\,\delta$ and $\Delta^{(\mathrm{RSD})}$ are included in standard analyses from spectroscopic surveys (e.g. DESI Collaboration: Adame et al., 2025),[1] with $\Delta_t^{(\mathrm{len})}$ appearing in the most recent analyses of photometric surveys (Dvornik et al., 2023; DES Collaboration: Abbott et al., 2025; Saraf et al., 2025). Finally, note that HI intensity mapping can also be described within the same formalism, where now t = HI labels the fluctuation in the mean temperature brightness of the 21-cm sky, $T_{\mathrm{HI}} = (1+\Delta_{\mathrm{HI}})\,\bar{T}_{\mathrm{HI}}$, and it is worth noting that in this case the lensing term identically vanishes, because surface brightness is conserved (see Hall et al., 2013, for an exhaustive treatment of relativistic effects in HI intensity mapping).

Cosmic shear and cross-correlations

The other main cosmological observable of the LSS is cosmic shear. Shear is one of the two components into which the amplification matrix of gravitational lensing can be decomposed, in

[1] Note that $\Delta^{(\mathrm{RSD})}$ is sample-independent and, as such, has no t subscript.

the weak lensing regime. Convergence is the other component. Shear acts on a galaxy image by stretching the image along one direction and contracting it in the orthogonal direction. Technically, it is characterized by a 2×2 traceless and symmetric tensor, whose two independent components, $\gamma_{i=1,2}$, can then be conveniently combined into a complex, spin-2 shear field, $\gamma = \gamma_1 + \mathrm{i}\,\gamma_2$. Analogously to CMB polarisation, we can introduce shear parity-eigenstates, called E- and B-modes, with the main advantages being: dealing with spin-0—and thus rotationally invariant—quantities; and allowing for a clean separation between cosmological signal and systematic effects—as, at linear order, B-modes cannot be generated in a parity-symmetric universe.

Cosmic shear is especially relevant in testing gravity because it is sourced by the Weyl potential, $\Upsilon \coloneqq (\Psi + \Phi)/2$, where Ψ is the gravitational potential that, together with the other metric potential Φ, forms the pair of gauge-invariant potentials (see Fig. 1). Lensing hence allows us to test modified gravity theories where the two potentials are not the same, unlike in GR (in the absence of anisotropic stress). Furthermore, cosmic shear is highly complementary to galaxy clustering, as the latter is mainly sensitive to Ψ alone, in the standard scenario. For this reason, weak lensing analyses usually consider the shear signal measured from galaxies jointly with their distribution, thus performing a so-called 3×2-point ('pt', for short) analysis, which includes shear-shear, galaxy-galaxy, and shear-galaxy correlations. It is worth remarking that relativistic effects contribute to cosmic shear only at second order (Bernardeau et al., 2010), whilst they impact lensing convergence already at linear order (Bacon et al., 2014), thus potentially affecting shear-galaxy correlations (Ghosh et al., 2018).

More generally, we shall refer to analyses of one single observable (e.g. shear-shear) as 'auto-correlations' and to those where the focus is on the interplay between two or more observables (like shear-galaxy) as 'cross-correlations'.

2.1 N-pt correlation functions and poly-spectra

Cosmological perturbations are stochastic and, as such, we can study their statistical properties. In particular, it is customary to define summary statistics in terms of moments of their probability distributions. Depending on whether we study perturbations in position (also, configuration) space or in some dual (e.g. Fourier) space, we shall refer to them as N-pt correlation functions or poly-spectra, respectively.

Cosmological perturbations are defined as fluctuations on top of a homogeneous and isotropic background. Hence, they average to zero, but their variance encodes information about their primordial distribution, as well as about the processes they underwent during the formation of the LSS (e.g. Peebles, 1980). The (co)variance of a cosmological field X at comoving position $\boldsymbol{r}$ and a (possibly different) field Y at position $\boldsymbol{r}'$ is called the 2-pt correlation function, which we denote by $\xi_{XY}(\boldsymbol{r}, \boldsymbol{r}') \coloneqq \langle X(\boldsymbol{r})\, Y(\boldsymbol{r}')\rangle$. In some cases, it is preferable to work in Fourier space, because on linear scales different Fourier modes evolve independently of each other. Thus, we define the power spectrum as the correlator of two perturbations in Fourier space, $\langle X(\boldsymbol{k})\, Y(\boldsymbol{k}')\rangle =: (2\,\pi)^3\, \delta_{\mathrm{D}}(\boldsymbol{k} + \boldsymbol{k}')\, P_{XY}(\boldsymbol{k})$, where δ_{D} is the Dirac-delta distribution and $\boldsymbol{k}$ and $\boldsymbol{k}'$ are Fourier wave-vectors—having used, with an abuse of notation, the same symbol for a configuration-space function and its Fourier transform.

A key assumption here is statistical homogeneity (translational invariance) in the local region where

we are correlating our N points (Zaroubi and Hoffman, 1993; Scoccimarro, 2015). However, as we correlate points at wide separations, this symmetry is broken. First, it is broken angularly, as we leave the plane-parallel limit, and as such, due to RSDs the points that we are correlating have different underlying statistics. Secondly, it is broken radially, due to the evolution of cosmological fields on the past light-cone. In Fourier poly-spectra we can introduce perturbative corrections in terms of the ratio between the distance to the two points, $\boldsymbol{d}$, and their separation, $\boldsymbol{s} = \boldsymbol{r} - \boldsymbol{r}'$, to account for some of this lost information when we assume translational invariance. These are the so-called wide-angle effects (Reimberg et al., 2016; Castorina and White, 2018; Noorikuhani and Scoccimarro, 2023) and radial-evolution corrections (Bonvin et al., 2014; Beutler and Di Dio, 2020; Paul et al., 2023; Addis et al., 2025).

To overcome this issue, a promising approach is to expand both fields in spherical Fourier-Bessel series, eventually dealing with a spherical power spectrum $C_l^{XY}(k, k')$, with now l representing an angular multipole and $k = |\boldsymbol{k}|$ and k' being Fourier wavenumbers (Castro et al., 2005; Rassat and Refregier, 2012; Yoo and Desjacques, 2013). This solution, however, is extremely computationally cumbersome (see e.g. Grasshorn Gebhardt and Doré, 2021), which is why it is more usual to expand only the angle between the lines of sight $\hat{\boldsymbol{r}} = \boldsymbol{r}/r$ and $\hat{\boldsymbol{r}}'$ in multipole series, keeping the configuration space positions in terms of the redshift corresponding to the radial comoving distances to the two perturbations, z and z'. Thus, we deal with the harmonic-space power spectrum, $C_l^{XY}(z, z')$, or its binned (a.k.a. tomographic) version, $C_{ij,l}^{XY}$, where now $i, j = 1 \ldots N_z$ label the N_z redshift bins which the original fields have been sliced into.

For a Gaussian random field—an ansatz that we believe is satisfied by the primordial gravitational potential—the mean and the variance are all that is needed to describe it. However, gravity is non-linear and density fluctuations that grew on top of those initial perturbations in the gravitational field to give rise to the observed LSS can no longer be described by Gaussian statistics. For this reason, we can also use higher-order correlators to study the LSS. Due to the increasing complexity of the problem, the most studied of such N-pt correlation functions is the 3-pt one, $\zeta_{XYZ}(\boldsymbol{r}_1, \boldsymbol{r}_2, \boldsymbol{r}_3) \coloneqq \langle X(\boldsymbol{r}_1)\, Y(\boldsymbol{r}_2)\, Z(\boldsymbol{r}_3)\rangle$, where now the three comoving positions form the vertices of a triangle. The corresponding poly-spectrum is the bispectrum, $\langle X(\boldsymbol{k}_1)\, Y(\boldsymbol{k}_2)\, Z(\boldsymbol{k}_3)\rangle =: (2\,\pi)^3\, \delta_{\rm D}(\boldsymbol{k}_1 + \boldsymbol{k}_2 + \boldsymbol{k}_3)\, B_{XYZ}(\boldsymbol{k}_1, \boldsymbol{k}_2)$, with the Dirac-delta ensuring momentum conservation in Fourier space.

As a last remark on nomenclature, we shall refer to auto- or cross- poly-spectra/N-pt correlation functions depending, respectively, on whether the N fields are all the same or not. Furthermore, if they are all analysed jointly, we shall refer to this as 'multi-tracing'.

3 Detecting relativistic effects in cosmological observables

This section is dedicated to prospects of detecting GR effects in the cosmological observables that will be measured by the SKAO. Any of such detections, which have drawn significant interest in the community over the past decade but have not yet been achieved, due to the elusiveness of relativistic effects, will serve as a further test of GR in the ultra-weak field regime. Since GR effects contribute to shear only at second order, as discussed in Section 2, it is then natural to focus on the clustering of tracers as a means to detect them.

3.1 2-pt correlations of galaxy number counts and intensity mapping

Cosmological information can be extracted from fluctuations in the number counts by measuring the 2-pt correlation function, $\xi_{tt'} \equiv \xi_{\Delta_t \Delta_{t'}}$ presented in Section 2.1. However, GR contributions to the observed Δ_t are strongest on the largest cosmic scales. The scarcity of independent modes for measurements of correlation functions on such scales—also known as cosmic variance—has hitherto hindered attempts at detecting GR effects. In this context, both the SKAO continuum galaxy survey (Asorey&Hale et al., 2026) and the SKAO HI intensity mapping surveys (Wolz et al., 2026), reaching up to the end of re-ionisation and deeper, will have access to enormous cosmological volumes, thus allowing us to access more modes even on those largest scales. Complementary to this, the SKAO HI galaxy survey (Nasirudin et al., 2026) will deliver a dense, low-redshift catalogue of sources, also suitable for studying relativistic effects thanks to the Doppler signal scaling with the ratio of the line-of-sight velocity to the Hubble expansion rate. This happens because, at low redshift, galaxy peculiar velocities are significant while the Hubble expansion rate is smaller, boosting the Doppler imprint in the observed clustering and thus making HI galaxies a promising tracer for these kinds of studies.

Another approach is to expand $\xi_{tt'}$ in Legendre multipoles about the angle $\hat{\boldsymbol{s}}$ separating the two lines of sight. Standard contributions to Δ_t, consisting of the density term and the RSD effect (see Eq. 1), generate a monopole, a quadrupole, and a hexadecapole. Relativistic contributions to these multipoles are highly subdominant (e.g. Jelic-Cizmek et al., 2021), but GR effects can also induce a dipole in the 2-pt correlation function and power spectrum (McDonald, 2009; Bonvin et al., 2014). However, for this dipole not to vanish it is essential to consider the cross-correlation between two different tracers, $t \neq t'$, with distinct properties. This can be achieved by cross-correlating any of the aforementioned radio tracers with others at different wavelengths or, in the case of HI and continuum galaxies, by splitting a parent sample into faint (t = F) and bright (t' = B) sub-samples. Figure 2 illustrates how such a split may create an asymmetry and thus a dipole in the galaxy correlation function.

Faint-bright cross-spectrum. We can subdivide the HI galaxy population into a faint and a bright sub-sample, and then measure cross-correlations between them. Following the procedure outlined in Montano and Camera (2024a,b), the left panel of Fig. 3 quantifies the relevance of the local relativistic corrections—whose main contribution comes from the Doppler term—in a measurement of the Fourier-space faint-bright cross-spectrum, $P_{\rm FB}(\boldsymbol{k})$, across the redshift range $z \in [0.1, 0.6]$. It assumes a surveyed area of 5 000 deg^2 (see SKA Cosmology SWG: Bacon et al., 2020), limited by the observation time, although SKAO's sky visibility could allow for a wider, more optimistic, coverage. The signal-to-noise ratio, SNR, depends on both the critical flux of the survey, $F_{\rm c}$, and the splitting flux between the two populations, $F_{\rm s}$. We can thus fix $F_{\rm s}$ in order to maximise the relativistic signal. The scaling of the detection significance versus the observed sky fraction, $\mathrm{SNR}(f_{\rm sky}) = \sqrt{f_{\rm sky}}\,\mathrm{SNR}(1)$, shows that a 15 000 to 20 000 deg^2 HI galaxy survey with AA4 specifications will reach a SNR ~ 2 with a measurement of the faint-bright cross-power spectrum alone. This, in turn, may lead to a robust detection of the relativistic Doppler effect by adding the constraining capability of auto-correlation Fourier-space spectra (following e.g. Montano and Camera, 2024b).

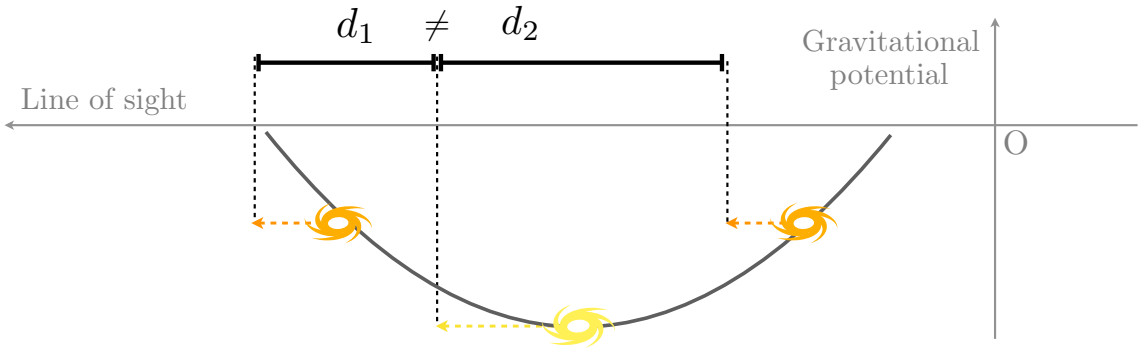

Figure 2: Gravitational redshift breaks the symmetry of 2-pt correlations, here illustrated by comparing three galaxies located in a gravitational potential. The brightest galaxy at the bottom of the potential is affected by the largest gravitational redshift, as its photons have to climb out of the deepest potential well to reach the observer at 'O' (middle right). The other two fainter galaxies are located at the same height in the potential and hence experience the same amount of gravitational redshift. Thus, in redshift space, the galaxies are shifted such that the central galaxy appears to be closer to the fainter galaxy behind than to the one in front. (Illustration adapted from Bonvin et al. 2014.)

Faint-bright multi-tracing. The two sub-samples can be seen as independent realisations of the same underlying matter density field, thus allowing for multi-tracer analyses (Seljak, 2009; McDonald and Seljak, 2009). Such a joint analysis of the auto-spectra $P_{\rm FF}$ and $P_{\rm BB}$, and the cross-spectrum $P_{\rm FB}$, will be able to limit cosmic variance and probe GR signatures with further precision (e.g. White et al., 2009; Abramo and Leonard, 2013; Alonso and Ferreira, 2015; Fonseca et al., 2015; Abramo et al., 2022). Thus, the right panel of Fig. 3 displays the statistical significance of $\Delta_t^{(\rm Dop)} \subset \Delta_t^{(\rm vel)}$ and $\Delta_t^{(\rm rel)}$, when probed by a multi-tracer faint-bright power spectrum, now considered in harmonic space. It essentially extends the outcomes of Novara et al. (2025) to the SKAO HI galaxy survey, showing that an optimal definition of the redshift bins will be able to counteract the loss of information due to the projection on spherical shells. Alongside, the flexibility in the binning choices may also be exploited to consider radio continuum galaxies (see Asorey&Hale et al., 2026). Although we found it unlikely to achieve a detection of relativistic Doppler with continuum galaxies, they may increase the constraining power of other targets, if cross-correlated with them.

Alternatively, one can consider the same type of faint-bright split approach but instead using the multipoles of the Fourier power spectrum, where one would use the so-called Yamamoto estimator (Yamamoto et al., 2006; Scoccimarro, 2015; Castorina and Di Dio, 2022). Figure 4 shows the constraints on the amplitude $\alpha_{\rm L}$ of the local relativistic terms and that of the integrated ones, $\alpha_{\rm I}$, in the scenario where one neglects wide-separation terms (dashed). As such, there is a shift in the best fit measurement of the amplitudes for a full multi-tracer analysis, as described in Addis et al. (2025). For this low redshift survey, the bias from wide-separation corrections is significant, amounting to as much as $\approx 15\,\sigma$. When we include wide-separation corrections, we also gain additional relativistic terms in the form of the wide-separation corrections to the relativistic contribution. Thus, we forecast a precise measurement of the local effects, $\sigma(\alpha_{\rm L}) = 0.12$, although the integrated effects themselves are unlikely to be detectable for this sample, $\sigma(\alpha_{\rm I}) = 3.2$. Note that here no

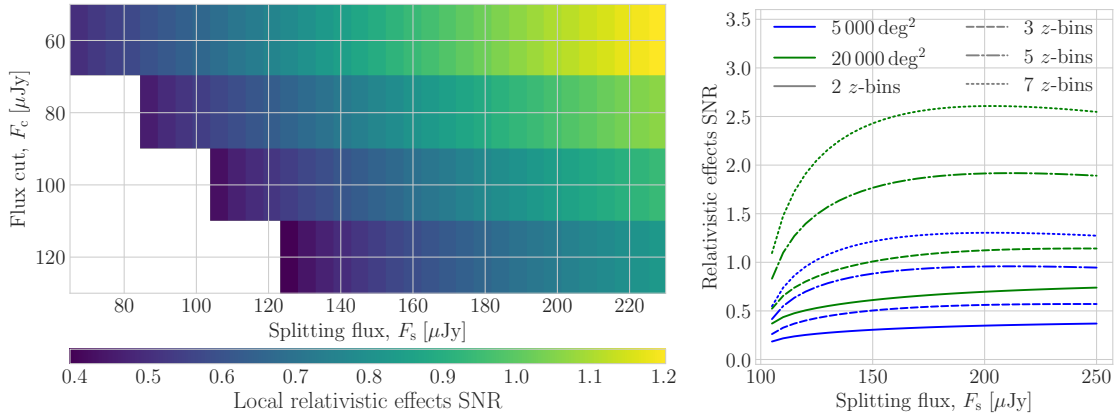

Figure 3: Cumulative SNR of the relativistic contributions in a faint-bright HI cross-spectrum, over the interval $0.1 \lesssim z \lesssim 0.6$. *Left:* In a $P_{\rm FB}(\boldsymbol{k})$ measurement, the SNR represents the statistical distance between data, affected by local GR effects, and a simple model which does not include relativistic corrections. *Right:* SNR, estimated via a null-hypothesis of $\Delta_t^{(\rm Dop)} = \Delta_t^{(\rm rel)} = 0$, in the case of a multi-tracer faint-bright angular power spectrum analysis. We assume a 100 µJy flux cut, together with both a conservative sky coverage of 5 000 deg^2 (blue curves) and an optimistic one of 20 000 deg^2 (green curves). Results in both panels illustrate how with an optimal choice of F_s we can boost the GR signal detection significance.

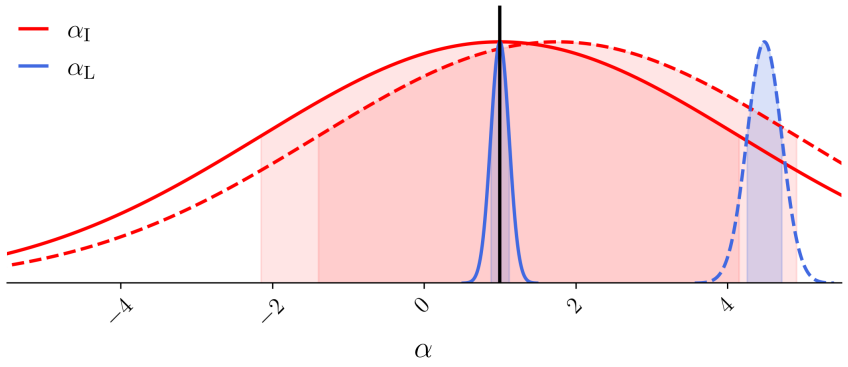

Figure 4: Forecast constraints on the amplitude of local and integrated relativistic contributions, α_L and α_I, in a multi-tracer analysis for the Legendre multipoles of the power spectrum (up to the hexadecapole), having included (solid lines) or not (dashed lines) wide-separation corrections in the theoretical model. We adopt a flux cut of $F_c = 100$ µJy and a $F_s = 150$ µJy splitting flux. The probability distributions are normalised to equal peak height, with the vertical black solid line marking the ground truth, $\alpha_L = \alpha_I = 1$.

uncertainty in the bias modelling is assumed.

Radio-optical cross-spectrum. The variety of LSS tracers provided by the SKAO allows for cross-correlations with traditional optical/near-infrared cosmological surveys over a broad swathe of redshifts. At high-z, HI intensity mapping can be analysed in cross-correlation with spectroscopic galaxy catalogues like *Euclid*'s or the DESI emission-line galaxy sample, with the advantage of negligible noise in the cross-spectrum. At lower redshift, we can exploit the almost perfect overlap between the high density of HI galaxies and the DESI bright galaxy sample.

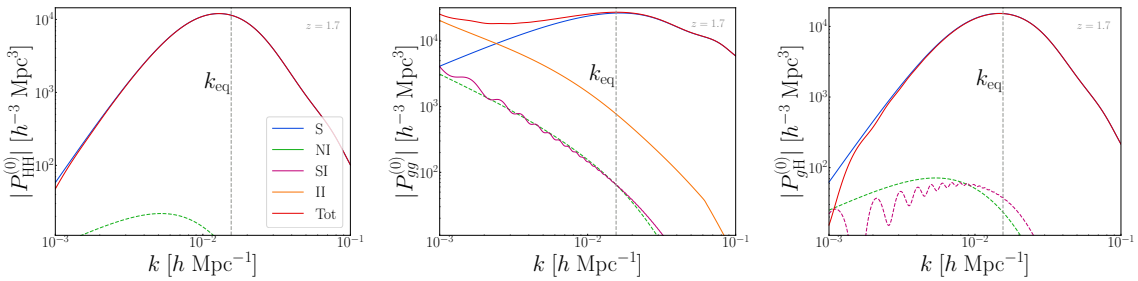

Figure 5: Legendre monopole of the SKAO HI-HI power spectrum (left panel), *Euclid* galaxy-galaxy power spectrum (middle panel), and their cross-spectrum (right panel) at $z = 1.7$. The plots display the importance of the non-integrated (NI), integrated (I), and total NI+I ('Tot') contributions, where I = SI + II.

Detecting the statistical effect of peculiar velocities would be crucial to understand how these are related to the gravitational potential Ψ, i.e. testing the Euler equation cosmologically. One can construct an anti-symmetric estimator (Bonvin and Fleury, 2018; Fonseca and Clarkson, 2021) on very large-scales that would be sensitive to the effect of peculiar velocities, i.e. the Doppler term, in the observed number counts of tracers of the LSS. The authors find that synergies between a catalogue of HI galaxies built from an AA* configuration and DESI can identify the Doppler term up to $3\,\sigma$, whilst only upgrades to the SKAO can deliver game-changing observations with radio observables alone in auto-correlation.

Regarding radio-optical synergies at high redshift, instead, we consider the SKA-Mid Band 1 intensity mapping survey and the *Euclid* Hα spectroscopic galaxy survey, both probing the LSS of the Universe in the redshift range $z \in [0.9, 1.8]$ and with an estimated overlapping sky area of approximately 8 000 deg^2. Figure 5, showing the Legendre monopole of the different power spectra at $z = 1.7$, demonstrates that relativistic integrated contributions ('SI', purple curves, and 'II', orange curves) are negligible for the HI auto-spectrum (left panel) and for the HI-galaxy cross-spectrum (middle panel), owing to the near cancellation of the lensing term in brightness temperature fluctuations. In contrast, in the *Euclid* galaxy auto-spectrum (right panel), the non-integrated corrections ('NI', green curves) become relevant at intermediate scales ($\sim 10^{-2}\,h\,\mathrm{Mpc}^{-1}$), while the integrated-integrated component dominates at ultra-large scales ($\sim 10^{-3}\,h\,\mathrm{Mpc}^{-1}$). This implies that the modelling of the HI power spectrum, already complicated on the largest scales because of the impact of foreground removal and signal loss (see e.g. Cunnington et al., 2023), as well as by imprints of inflationary physics (Cunnington et al., 2020), is not expected to be affected by neglecting a precise modelling of relativistic effects.

3.2 Bispectrum of galaxy number counts and intensity mapping

The dominant relativistic signature in galaxy clustering, the Doppler correction, can be best exposed in the 2-pt correlation function and power spectrum only when considering cross-correlations. The bispectrum, on the other hand, provides a powerful complementary approach: a 'smoking gun' imaginary dipole signal is accessible in the bispectrum of a single tracer, without the need for cross-correlations (Clarkson et al., 2019; Jeong and Schmidt, 2020). This also applies to HI intensity mapping (Jolicoeur et al., 2021). Higher-order statistics such as the 4-pt correlation function also contain these signatures (Paul et al., 2024), extending the treatment of relativistic effects in the

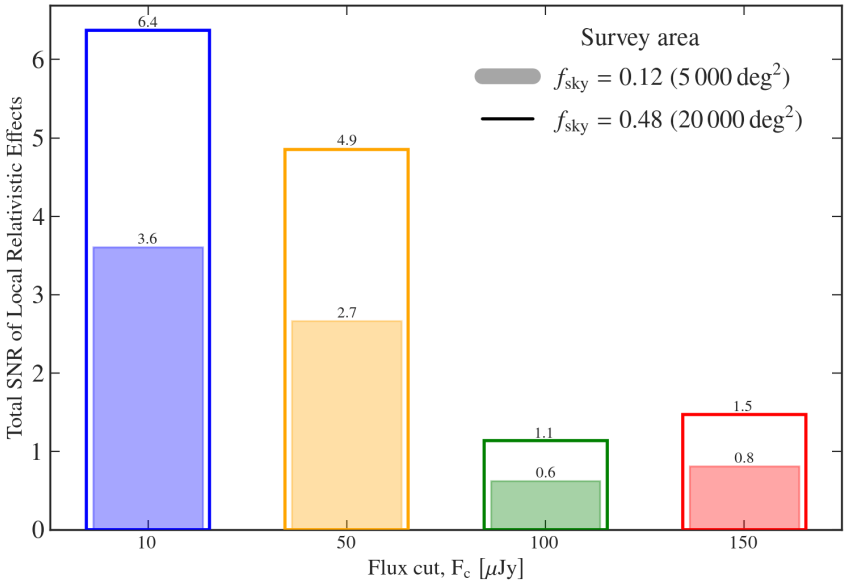

Figure 6: The forecasted cumulative signal-to-noise ratio of the relativistic contributions to the galaxy bispectrum for SKAO HI galaxies, assessed at various flux cuts. For more realistic flux cuts, 150 µJy and 100 µJy, the signal is unlikely to be detectable. Future improvements to the flux sensitivity of the instrument could prove fruitful in this regard.

non-linear regime, generalising Eq. (1).

However, detecting such contributions using the auto-bispectrum remains inherently challenging as we fight against the limited number of large-scale modes and noise in this range. Figure 6 presents forecasts for the cumulative signal-to-noise ratio associated with the general relativistic contributions to the galaxy bispectrum for SKAO HI galaxies. We assess the expected sensitivity achievable with the single-tracer bispectrum and establish a baseline for future improvements aimed at maximising scientific return of SKAO on ultra-large scales. In fact, as we see in Fig. 6, the scientific return can be optimised by varying the flux cut of the sample. Whereas lower flux cuts generally improve the signal-to-noise ratio by increasing the number density, the behaviour at high flux cuts ($F_c \approx 150$ µJy to 100 µJy) is non-monotonic: the bispectrum covariance is shot-noise dominated, thus the noise penalty saturates. In this regime, enhancements from magnification and evolution bias—particularly at intermediate to high redshifts—outweigh the additional noise contribution. A full multi-tracer bispectrum can exploit this further (Rossiter et al., 2026). These results mark an initial step in exploiting the full potential of the clustering of HI galaxies to test gravity.

Moreover, an important motivation for studying the bispectrum is its role in detecting primordial non-Gaussianity (PNG) via the scale-dependent bias that local PNG induces (see also Fonseca et al., 2026). On ultra-large scales, however, relativistic terms generate scale-dependent signatures that closely resemble those sourced by local PNG (Bruni et al., 2012; Camera et al., 2015; Maartens et al., 2021). If unaccounted for, these relativistic contributions can bias measurements of the local PNG amplitude, f_{NL} (Umeh et al., 2017; Di Dio et al., 2017; Rossiter et al., 2024; Addis et al.,

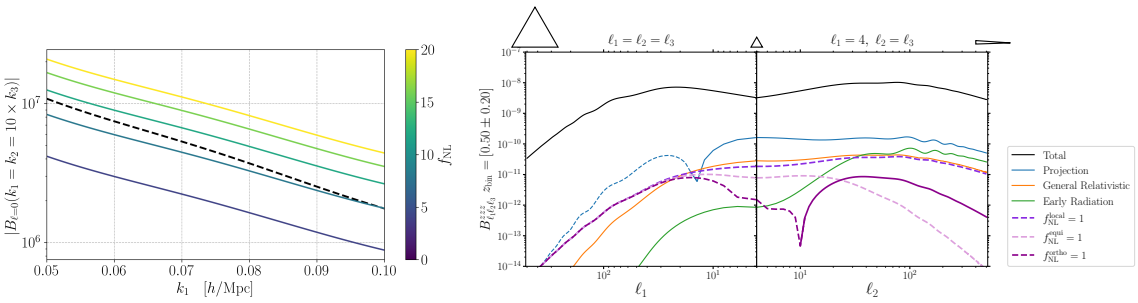

Figure 7: Bispectrum of SKAO HI galaxies including both GR contributions and PNG, in both Fourier and harmonic space (left and right panel, respectively). Coloured lines in the right panel refer to different values of the PNG amplitude parameter, $f_{\rm NL}$, with the GR prediction being the black, dashed curve. In the left panel, the total GR bispectrum (solid black) is compared to the Newtonian approximation (dotted black), with individual relativistic contributions shown: relativistic projection effects (blue), GR corrections (orange), and early-time radiation effects (green). Long-dashed purple lines show the PNG signals for local (dark), equilateral (light), and orthogonal (medium) shapes with $f_{\rm NL} = 1$. Triangle diagrams at the top illustrate the respective configurations. Solid and short-dashed curves respectively refer to positive or negative bispectra.

2025). To illustrate this interplay between relativistic effects and PNG in the bispectrum, we present in Fig. 7 the bispectrum of SKAO HI galaxies, both in Fourier space (left panel) and in harmonic space (right panel). For the former, we show the local-type PNG signal in a squeezed limit of the Legendre monopole of the bispectrum for different values of the PNG amplitude parameter $f_{\rm NL}$, in comparison to the local relativistic signal (black dashed), assuming a nominal 100 μJy flux cut. Clearly, the scale dependence of the PNG signal closely resembles that of GR effects.

Similarly, in the right panel we see the harmonic-space bispectrum, $B^{zzz}_{\ell_1\ell_2\ell_3}$, again for an SKAO HI galaxy survey in a redshift bin centred on 0.50 and of width 0.20.[2] In this framework, all types of local and integrated GR terms can be easily introduced (Di Dio et al., 2014, 2016, 2019; Assassi et al., 2017; Montandon et al., 2023, 2025). Here, we can compare the full GR prediction with its Newtonian approximation across two configurations: equilateral ($\ell_1 = \ell_2 = \ell_3$) in the left panel (with reverted abscissas) and squeezed ($\ell_1 = 4$, $\ell_2 = \ell_3$) in the right panel. Solid(dashed) curves represent positive(negative) bispectra. The relativistic projection effects, also sourcing the bispectrum dipole, peak at large scales in the equilateral configuration, where they represent 10% of the signal. In the squeezed limit, they constitute the dominant relativistic contribution. Crucially, the relativistic signatures exhibit amplitude and angular scale dependence similar to that of PNG, highlighting the degeneracy challenge: neglecting relativistic effects when constraining $f_{\rm NL}$ could lead to significant biases.

However, this also presents an opportunity: by modelling both contributions simultaneously, the bispectrum offers a means to constrain inflationary physics and test GR on cosmological scales. Thus, the relativistic bispectrum provides an additional avenue to test gravity on cosmological scales in addition to the power spectrum and 2-pt correlation function, with the added benefit of directly mitigating biases in the constraints on inflationary models.

[2]The angular bispectrum of galaxy count is evaluated using the code `ang_bispec` (Montandon et al., 2025).

4 Detecting signatures of modified gravity

The idea behind modified gravity theories is to alter the gravitational dynamics on large scales, comparable to or greater than the Hubble radius, whilst preserving the successful predictions of GR on Solar System and smaller scales. This can be achieved through several mechanisms. The best-studied examples are scalar-tensor theories, such as Horndeski, beyond-Horndeski, and DHOST models, which introduce one additional scalar degree of freedom coupled to the metric and modify both the propagation of gravitational waves and the effective gravitational constant (Horndeski, 1974; Deffayet et al., 2011; Langlois and Noui, 2016).

However, other field contents are also viable. Tensor-tensor theories (e.g. bimetric gravity) introduce an additional dynamical metric, leading to massive graviton degrees of freedom (Hassan and Rosen, 2012). Vector-tensor theories, such as generalized Proca or Einstein-Æther models, introduce vector fields that can drive the acceleration or modify the growth of structure (Heisenberg, 2014; Jacobson, 2007). Non-metric theories, including teleparallel gravity or symmetric teleparallel $f(Q)$ models (Beltrán Jiménez et al., 2019), reformulate gravitation in terms of torsion or non-metricity instead of curvature, offering geometrically distinct routes to cosmic acceleration.

To remain consistent with local and astrophysical tests, many of these theories rely on screening mechanisms (chameleon, Vainshtein, or symmetron effects) that suppress deviations from GR in high-density environments (see Khoury and Weltman, 2004; Babichev and Deffayet, 2013). The rich phenomenology of these frameworks, ranging from modified GW speed to scale- and/or time-dependent effective couplings, opens multiple observational windows for testing gravity on cosmological scales. At the cost of limiting constraints to insights on specific models, HI intensity mapping over large SKAO-like volumes is, for example, expected to be sensitive to the shape of scalar potentials and effective couplings, as has been shown for redshift $z > 6$ (Liu et al., 2020).

In addition to exploring specific models, an important complementary strategy involves model-independent parametrisations of cosmic acceleration. The effective field theory (EFT) of dark energy and modified gravity provides a unified framework that captures the low-energy dynamics of a wide class of single scalar field modified gravity and dark energy models in terms of a finite set of time-dependent functions appearing in the perturbed action (Frusciante and Perenon, 2020). This approach allows for a systematic comparison between theory and data without committing to a specific Lagrangian.

From an SKAO perspective, a MeerKLASS-like HI intensity mapping survey would improve the constraints on the EFT functions with respect to *Planck*'s current bounds (Berti et al., 2022). Figure 8 shows the results for an EFT model described by a running of the gravitational constant (namely, of the Planck mass) that evolves exponentially with the scale factor, i.e. $\Omega^{\rm EFT}(a) = \exp(\Omega_0^{\rm EFT} a^\beta) - 1$. The constraints presented are obtained by combining the forecast MeerKLASS-like data sets with *Planck* 2018 observations. Whilst the power-law index β is left almost unconstrained, we observe that HI intensity mapping tomography will tighten the error bar on $\Omega_0^{\rm EFT}$ by $\sim 25\%$ with respect to *Planck* alone. Furthermore, if e.g. observation time could be extended so as to halve instrumental noise errors, the increment would go up to $\sim 35\%$. Instead, the constraining power of single-bin observations is insufficient to improve upon *Planck*'s results.

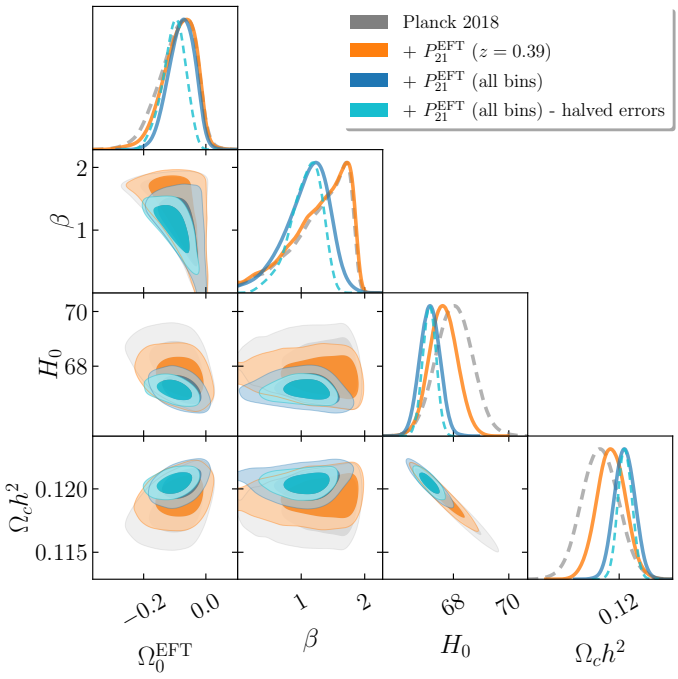

Figure 8: Results from Berti et al. (2022). Forecast joint constraints on parameters of EFT models of dark energy from a MeerKLASS-like HI intensity mapping survey in combination with *Planck* 2018 data. We compare the constraining power of a single bin HI auto-spectrum detection ($z = 0.39$) with a five-bin one, at $z = 0$, 0.39, 0.53, 0.67, 2.5 ('all bins' in legend). We also consider a more ideal case with smaller errors. The label *Planck* 2018 stands for TT, TE, EE + lowE + lensing.

It is also possible to constrain dark energy models with HI intensity mapping observations alone, but using other experiments in different redshift intervals, provided that there is an excellent foreground removal (Wu and Zhang, 2022; Wu et al., 2023). In particular, with SKA-Mid ($0.35 < z < 0.8$), the errors on the parameters of ΛCDM—with an equation-of-state parameter for dark energy different from a cosmological constant—are lower than those obtained by current measurements from *Planck* in combination with baryon acoustic oscillations and type Ia supernovæ. This happens because different parameter degeneracies are lifted by such probe combinations. In addition, this strategy can significantly improve constraints on the Hubble constant H_0 and on the cosmographic parameters q_0, j_0, and s_0, which are phenomenological direct tests of the deviation of dark energy from the ΛCDM model (see also Section 5). Another model independent approach may involve an effective dark fluid equation of state parameter that encapsulates modified gravity theories that alter both the Universe's background expansion and the growth of the LSS, for which SKAO observations in combination with surveys such as *Euclid* appear promising (e.g. Sakr, 2026).

Phenomenological parametrisations of modified gravity, on the other hand, offer a more direct connection to observables: the modified Poisson equation and lensing potential can be expressed through the functions $\mu(a, k)$ and $\eta(a, k)$, as depicted in Fig. 1, which respectively describe modifications to the clustering of matter and to light deflection (Zhang et al., 2007; Amendola et al., 2008; Pogosian et al., 2010). Deviations from GR would appear as scale- and/or redshift-dependent

departures of these functions from unity, which represents their GR limit. These functions are more naturally defined in Fourier space rather than configuration space in order to preserve statistical homogeneity. This is the convention that we adopt in the following to compare with mainstream literature on the topic.[3]

Constraints on μ and $\Sigma = (1+\eta)\,\mu/2$ from SKAO HI and continuum galaxy clustering and radio cosmic shear, in combination with optical/near-infrared probes, have been shown to be very competitive (Casas et al., 2023), with constraints ranging from 0.83% to 2.55% on μ and from 0.55% to 1.2% on Σ. Similarly, HI intensity mapping is able to constrain μ over a wide range in redshift (and scale), with similar percent-level constraining power also expected at redshifts higher than those of large-scale galaxy surveys (Heneka and Amendola, 2018).

Lastly, another widely used diagnostic to detect deviations from GR is the growth index, γ, which parameterises the growth rate of cosmic structures as $f(a) = [\Omega_{\rm m}(a)]^{\gamma}$. GR with a cosmological constant—that is, ΛCDM—predicts $\gamma \simeq 0.55$, whilst modified gravity theories generally predict different values or redshift dependencies (Linder, 2005). This framework allows for data-driven reconstruction of the gravitational interaction and serves as a key tool in forthcoming analyses of the LSS. Viljoen et al. (2020) proposed studying the growth index γ by using the angular power spectrum of SKAO HI galaxies, as it naturally includes the Doppler effect and gravitational lensing and does not require correcting for the Alcock-Paczyński effect. Combining SKA1 with DESI or *Euclid*, it is possible to reach an accuracy of $\sim 2\%$ on γ (see also Dlamini et al., 2024, for a multi-tracer approach). Moreover, by using the bispectrum in combination with the HI intensity mapping power spectrum, sub-percent precision on ΛCDM parameters can be attained, in an extended parameter space including γ as well as the dark energy equation-of-state parameters w_0 and w_a (Karagiannis et al., 2022).

5 Additional probes of gravity

Hitherto, we have focussed on the most widely employed techniques to probe the LSS, viz. the summary statistics introduced in Section 2.1. In this section, instead, we present other promising probes, whilst keeping a clear SKAO perspective. For instance, the survey capabilities of the SKA-Mid, tracing redshifts of HI galaxies and the variations in continuum brightness over cosmic time, enable a measurement of redshift drift (Klöckner et al., 2015), mapping the expansion history of the Universe in a model-independent way (Sandage, 1962). The expected signal is a velocity shift of a few $\mathrm{cm\,s^{-1}}$ over a timescale of approximately a decade. This requires precise determination of the line-centre offset of the averaged HI emission line profile. A key factor is the number of HI galaxies used in the stacking process.

To estimate uncertainties in the line-centre offset, we assume that individual HI emission lines are Gaussian distributed with no significant technical systematics. The uncertainty in the redshift drift

[3] In the presence of a non-trivial scale-dependence, the conversion to configuration space leads to a less convenient form of the Poisson equation involving a convolution with a non-local derivative operator, so that the gravitational potential at one point depends on the density field at other points. There are however specific cases where a configuration-space definition is more suitable, for example in the presence of screening effects, where the modifications are non-perturbative and environment-dependent.

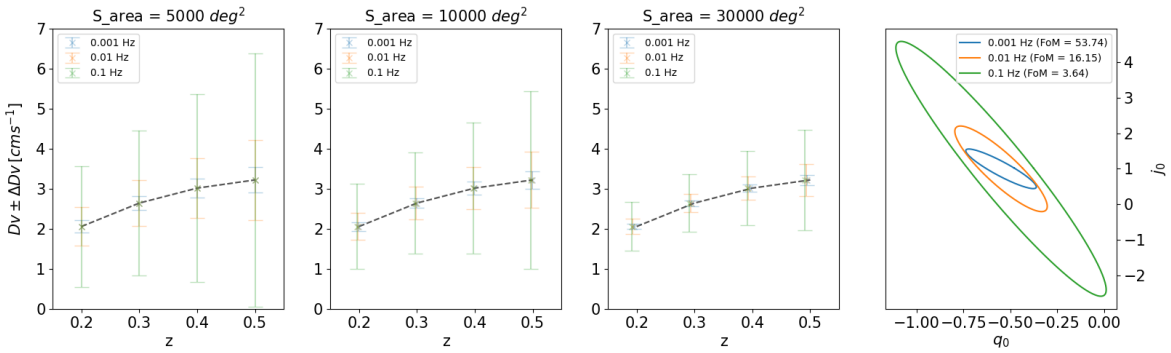

Figure 9: *Left plots:* Theoretical prediction and error estimates of the redshift drift versus redshift, for different channel width (0.001, 0.01, and 0.1 Hz) and survey areas (5 000, 10 000, and 30 000 deg^2). *Rightmost plot:* Confidence regions for the cosmographic deceleration, and jerk parameters, assuming a prior in the marginalized Hubble constant, for the same choices of channel width and survey area of 5 000 deg^2.

can then be described by the error in the line centre of a Gaussian profile (Minin and Kamalabadi, 2009, Eq. 14), weighted by the square root of the number of stacked spectra. Figure 9 (three panels from the left) shows the expected redshift drift in units of cm s^{-1} within twelve years, with estimated SKA-Mid AA* errors for several choices of channel width and sky coverage, assuming one hour of observation per pointing. Even with a moderate sky coverage of 5 000 deg^2 and a survey duration of approximately six months, a redshift-drift experiment is within reach of the SKA-Mid AA*. Here, the average uncertainty in the HI-line is fixed to 150 km s^{-1} (SAX simulations, Obreschkow et al., 2009), whilst the angular number density of HI galaxies uses the updated functional description of the number densities of Yahya et al. (2015). We further assume single-channel detections from previous large-sky surveys. The values of the MPA are defined by the flux-density boundaries given in Yahya et al. (2015).

Constraints from these measurements can be forecast using information matrix analysis tools (Alves et al., 2019; Rocha and Martins, 2022; Marques et al., 2023), which directly constrain the cosmographic series up to the jerk parameter, i.e. H_0, q_0, and j_0 (see also Section 4). With a conservative prior $\sigma(H_0) = 10\,\mathrm{km\,s^{-1}\,Mpc^{-1}}$, constraints in the (q_0, j_0)-plane are presented in the rightmost panel of Fig. 9, including a figure of merit (FoM), defined as the inverse of the area of the one-sigma confidence ellipse. We use the publicly available `FRIDDA` code and assume three redshift bins centred at 0.1, 0.3, and 0.5, considering velocity uncertainties corresponding to the scenarios in Fig. 9. We find one-sigma uncertainties for q_0 and j_0 ranging from 0.65 to 0.08 and from 4.2 to 0.25 respectively. This shows that with a reasonable investment of observing time, SKA-Mid AA* can deliver meaningful model-independent constraints. The best-fit concordance model yields model-dependent predictions for them, to be compared to these observations, validating or excluding the model. Such early observations will also clarify technical requirements, identify systematic bottlenecks, and optimize subsequent observational strategies. Since the redshift drift signal grows linearly with time, the precision of such measurements will improve with extended observational baselines, making SKA-Mid a powerful tool for future cosmographic studies.

Furthermore, gravity theories can also be tested through gravitational wave observations. The

detection of polarisation modes other than the two tensor modes may signal deviations from Einstein's theory of gravity (Eardley et al., 1973a,b). Moreover, these modes can be frequency-dependent (Hyun et al., 2019), and modified gravity models can accommodate parity violation features such as amplitude and velocity birefringence effects in their dispersion relations. In fact, the ripples in the fabric of spacetime exist across a range of frequencies, or wavelengths. Low-frequency gravitational wave signals can form a stochastic background and originate either from the mergers of supermassive black hole binaries or from early time processes such as the ones which can arise from inflationary processes including the reheating and preheating periods where cosmological phase transitions can occur. These signals produce a distinctive signature, namely they show a quadrupolar spatial correlation between the arrival time of pulses emitted by different millisecond pulsar pairs, associated with the Hellings-Downs curve (Hellings and Downs, 1983). These millisecond pulsars are not likely to be sensitive to starquakes and glitches, thus acting as stable astrophysical clocks and reliable laboratories to test GWs (Verbiest et al., 2021). Therefore, scientific missions using pulsar timing techniques have been implemented.

The SKAO will reach peaks of sensitivity higher than those of current pulsar timing array experiments, such as the International Pulsar Timing Array consortium (Perera et al., 2019). Moreover, it will enable probes of the stochastic gravitational wave background and searches for individual supermassive black hole binaries. This complements other ground- and space-based GW experiments, such as the ET (Abac et al., 2025a), the LIGO-Virgo-Kagra Collaboration (Abac et al., 2025b), and LISA (Auclair et al., 2023). This wide range of frequencies covered by these observatories will provide insights into the nature of gravity, as most of these experiments and the GW sources they probe do not overlap, hence the information extracted from each will be different and complementary.

6 Future perspectives

A future upgrade of the SKAO, often referred to as 'Phase 2' of the SKAO, will enable additional tests of fundamental physics on cosmological scales (e.g. Weltman et al., 2020). Thanks to the increased statistics in the number of spectroscopically observed HI-galaxies, it will provide sensitivity to GR effects in the clustering signal. As discussed in Section 3, these effects generate a dipole term in the two-point correlation function of galaxies, which is expected to be detectable with a signal-to-noise of around 80 by Phase 2 of the SKAO (Castello et al., 2024a).

One of these GR effects is gravitational redshift, which corresponds to the frequency change of photons crossing gravitational potential differences. As such, this effect is directly sensitive to the time distortion Ψ, hence giving access to one of the four fundamental fields in Fig. 1 and providing crucial information for testing the properties of gravity and dark matter on cosmological scales. To achieve this, gravitational redshift can be combined with RSDs, which probe peculiar velocities V, and weak gravitational lensing, which is sensitive to the sum of the two potentials $\Phi + \Psi$. In the following, we illustrate the new tests that can be performed with these combinations of observables.

RSDs have been used to constrain modifications to the Poisson equation parametrised through the phenomenological function μ in Fig. 1 (see e.g. Alam et al., 2021). Such constraints are obtained

by employing the Euler equation to relate the peculiar velocities measured from the RSDs to the time distortion Ψ, which can then be combined with measurements of the density δ from galaxy clustering, as per Fig. 1. However, Castello et al. (2022) (see also Bonvin and Pogosian 2023; Castello et al. 2024b) showed that this approach is affected by a dangerous shortcoming, as it relies on the restrictive assumption that CDM obeys the weak equivalence principle, encoded in the Euler equation. Physically, this corresponds to the statement that CDM falls into gravitational potentials in the same way as ordinary matter, which has not been proven to date and does not hold in several extended dark matter models. This could be due to gravity coupling differently to different matter species (e.g. Gleyzes et al., 2015) or arising as an effective violation due to non-gravitational interactions of CDM with Standard-Model particles (e.g. Barkana, 2018) or within the dark sector (Pourtsidou et al., 2013; Spergel and Steinhardt, 2000; Tulin and Yu, 2018).

However, without the restrictive assumption of the weak equivalence principle, RSD analyses show a strong degeneracy between the function μ in the Poisson equation and modifications to the Euler equation (Castello et al., 2022). Such modifications can be parameterised with two additional time- and scale-dependent phenomenological functions: Θ and Γ in Fig. 1, representing a fifth force and a friction term acting on CDM, respectively (Bonvin and Fleury, 2018). By probing the growth rate of cosmic structure, RSD surveys can only constrain the fully degenerate combination $\mu + \Gamma$ and thus cannot distinguish between the effect of μ, encoding the depth of gravitational potentials, and that of Γ, controlling how CDM falls into these potentials. Such modifications can have the very same impact on the evolution of cosmic structure. Additionally, there is a strong degeneracy with the friction term Θ, leading to a severe widening of the joint constraint on $\mu + \Gamma$.

Luckily, including measurements of gravitational redshift from SKAO Phase 2 efficiently lifts this degeneracy, leading to tight individual constraints on gravity modifications and violations of the weak equivalence principle. Notably, the value of μ at present time is forecasted to be constrained at the level of 14.7%, exceeding the precision of current RSD constraints obtained under the limiting assumption that the weak equivalence principle is valid (Alam et al., 2021). This remarkable result is motivated by the fact that gravitational redshift provides complementary information to RSDs, as it probes how photons escape from a gravitational potential, while RSDs are sensitive to the growth of matter perturbations. This is crucial to disentangle modified gravity from extended CDM scenarios where the weak equivalence principle is broken, which would otherwise be completely indistinguishable in a standard RSD analysis (Bonvin and Pogosian, 2023; Castello et al., 2024b).

Castello et al. (2024a) further demonstrated the constraining power of gravitational redshift with a complementary approach, based on theoretically motivated parameters. This analysis was performed within the framework of the effective theory of interacting dark energy, a broad class of extended models covering the full set of Horndeski theories and at the same time allowing for different couplings of the cosmic components to gravity. Also in this case, the inclusion of gravitational redshift in the forecasts for the SKAO Phase 2 leads to a clear breaking of degeneracies in the parameter space and improvements in the constraints of up to 50%.

The combination of RSDs and gravitational redshift also provides a direct test of the Euler equation by linking Ψ to V, as can be seen from Fig. 1. Castello et al. (2025) developed a model-independent null test E_P that deviates from 1 in the presence of a violation, which relies on minimal assumptions

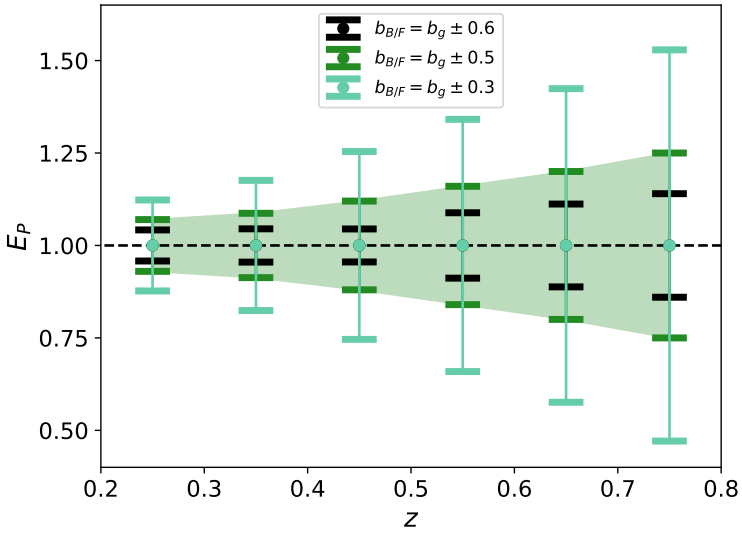

Figure 10: Constraints on deviations from the weak equivalence principle from SKAO Phase 2, encoded in the deviation of the parameter E_P from 1 as a function of redshift. The colours correspond to various bias differences between the two galaxy populations (bright B and faint F) considered to detect the dipole in the 2-pt correlation function, which is sensitive to GR effects as discussed in Section 3. Larger bias differences improve the detection significance and hence the constraints. (Reproduced from Castello et al. 2025.)

and in particular does not require specifying the power spectrum shape, the background evolution, the growth rate of cosmic structure, the galaxy bias or a model for the potential violation of the equivalence principle. Forecasts for SKAO Phase 2 indicated expected constraints around 10–15% as a function of redshift, as shown in Fig. 10.

Although gravitational redshift with SKAO Phase 2 will give us access to the time distortion Ψ, weak lensing surveys provide highly complementary information, as they are sensitive to the sum $\Phi + \Psi$. As suggested in Sobral-Blanco and Bonvin (2021) and further explored in Tutusaus et al. (2023), the combination of gravitational redshift and lensing can thus be exploited to constrain anisotropic stress, defined as the ratio $\eta \equiv \Phi/\Psi$. This presents a direct comparison of the two metric degrees of freedom, which are predicted to be equal if general relativity holds. As such, it is a key test of the governing theory of gravity. Tutusaus et al. (2023) has found that, with a combination of gravitational redshift from SKAO Phase 2 and gravitational lensing from LSST, the quantity $2/(1+\eta)$ can be constrained at the level of $\sim$ 20% in an optimistic scenario (and $\sim$ 30% in the pessimistic case). This constraint is obtained in a model-independent manner, directly comparing the two metric components without relying on assumptions such as the validity of the weak equivalence principle.

7 Conclusions

The coming decade will see a step change in our ability to test gravity on cosmological scales, the SKAO playing a central role. By mapping HI-line and radio-continuum galaxies over huge comoving

volumes and a broad redshift range, the SKAO will probe both the background expansion and the growth of structure in a way that is highly complementary to optical/near-infrared observations and CMB surveys. Within the ΛCDM framework, this will allow for stringent internal consistency tests: does a single relativistic model, with a small set of parameters, account simultaneously for baryon acoustic oscillations, RSDs, weak lensing, and higher-order clustering across radio, optical and microwave data sets? A positive answer would significantly strengthen the status of GR+ΛCDM as an effective theory on ultra-large scales; a negative answer would help localise where the standard picture fails, whether in the expansion history, in the growth of perturbations, or in the relativistic projection effects that link theory to observables.

A key theme of this chapter has been the role of intrinsically relativistic effects in LSS observables (Section 3). These have traditionally been treated as small 'corrections' to Newtonian analyses, lying just beyond the reach of current data. SKAO surveys will change this situation. The combination of very large survey volumes, multi-tracer strategies (e.g. faint-bright splits, radio-optical cross-correlations), and measurements in both configuration and Fourier space opens up realistic prospects for detecting Doppler terms, gravitational redshift signatures, lensing magnification, and other light-cone effects. These signals are not merely nuisances to be modelled away: they are direct tests of GR in the ultra-weak field regime. At the same time, a robust treatment of these terms will be essential for unbiased constraints on PNG and on any scale-dependent deviations from the standard picture.

Beyond testing GR, the SKAO will provide a powerful laboratory for alternatives and extensions to the ΛCDM model (Section 4). Model-independent frameworks such as the effective field theory of dark energy and phenomenological parameterisations of modified gravity (e.g. μ, η, Σ, and the growth index γ) offer a common language in which SKAO measurements can be confronted with those from *Planck*, *Euclid*, DESI, LSST, and future CMB experiments. HI intensity mapping and radio galaxy clustering will sharpen constraints on the time and scale dependence of the effective gravitational coupling and lensing potential, while higher-order statistics (bispectra and beyond) will help to disentangle relativistic projection effects from primordial signatures such as local $f_{\rm NL}$.

Looking ahead, Phase 2 of the SKAO (Section 6) will extend these capabilities substantially, turning several of the forecasts in this chapter into precision tests. A high-significance detection of the relativistic dipole in the 2- and 3-point correlation functions, direct constraints on gravitational redshift and anisotropic stress, and model-independent tests of the Euler equation and the weak equivalence principle become realistic targets. In combination with optical, infrared, CMB and gravitational-wave facilities, the SKAO will allow us to improve significantly on standard cosmological gravity tests: either reinforcing GR+ΛCDM as an excellent effective description across a wide dynamical range or providing clear signposts towards new physics in the dark sector or in the law of gravity itself. In either outcome, radio cosmology with the SKAO will be central to our attempt to understand the origin of cosmic acceleration and the behaviour of gravity on the largest scales accessible to observation.

Author List Ordering

Authors for this chapter are ordered as: corresponding author, alphabetical tiers. Authors in the first tier contributed to the chapter by producing original results using SKAO updated specifications. The second tier comprises authors who wrote significant part of the text and/or provided necessary inputs for the analysis. Authors in the last tier contributed with useful comments and constructive feedback, active supervision, and valuable inputs for discussion.

Acknowledgments

StC, SJR, and FM acknowledge support from the Italian Ministry of University and Research (MUR), PRIN 2022 'EXSKALIBUR – Euclid-Cross-SKA: Likelihood Inference Building for Universe's Research', Grant No. 20222BBYB9, CUP D53D2300252 0006, from the Italian Ministry of Foreign Affairs and International Cooperation (MAECI), Grant No. ZA23GR03, and from the European Union – Next Generation EU. TM is supported by funding from the European Research Council (ERC) under the European Union's HORIZON-ERC-2022 (Grant No. 101076865). SvC, NG, and CB acknowledge funding from the European Research Council (ERC) under the European Union's Horizon 2020 research and innovation program (Grant No. 863929; project title "Testing the law of gravity with novel large-scale structure observables"). SvC is supported by a Postdoc Mobility Fellowship of the Swiss National Science Foundation (SNSF), project No. P500PT 230281. NG is supported by the STFC, Grant No. ST/B001175/1. SLG and RM are supported by the South African Radio Astronomy Observatory and the National Research Foundation, Grant No. 75415. CH's work is funded by the Volkswagen Foundation. This work was supported by the DFG under Germany's Excellence Strategy EXC 2181/1 – 390900948 The Heidelberg STRUCTURES Excellence Cluster. This work was financed by Portuguese funds through FCT (Fundação para a Ciência e a Tecnologia) in the framework of the project 2022.04048.PTDC (Phi in the Sky, DOI 10.54499/2022.04048.PTDC). CJAPM also acknowledges FCT and POCH/FSE (EC) support through Investigador FCT Contract 2021.01214.CEECIND/CP1658/CT0001 (DOI 10.54499/2021.01214.CEECIND/CP1658/CT0001). ZS acknowledges support from the research projects PID2021-123012NB-C43, PID2024-159420NB-C43, the Proyecto de Investigación SAFE 25003 from the Consejo Superior de Investigaciones Científicas (CSIC), and the Spanish Research Agency (Agencia Estatal de Investigación) through the Grant IFT Centro de Excelencia Severo Ochoa No. CEX2020-001007-S, funded by MCIN/AEI/10.13039/501100011033.

References

A. Abac et al. 3 2025a.

A. G. Abac et al. 8 2025b.

L. R. Abramo and K. E. Leonard. Mon. Not. R. Astron. Soc., 432(1):318–326, Apr. 2013. ISSN 1365-2966. doi: 10.1093/mnras/stt465. URL http://dx.doi.org/10.1093/mnras/stt465.

L. R. Abramo, J. V. D. Ferri, and I. L. Tashiro. J. Cosmol. Astropart. Phys., 2022(04):013, Apr. 2022. ISSN 1475-7516. doi: 10.1088/1475-7516/2022/04/013. URL http://dx.doi.org/10.1088/1475-7516/2022/04/013.

C. Addis, C. Guandalin, and C. Clarkson. J. Cosmol. Astropart. Phys., 2025(4):080, Apr. 2025. doi: 10.1088/1475-7516/2025/04/080.

C. Addis et al. 2025. URL https://arxiv.org/abs/2511.09466.

S. Alam et al. Phys. Rev. D, 103(8):083533, 2021. doi: 10.1103/PhysRevD.103.083533.

D. Alonso and P. G. Ferreira. Phys. Rev. D, 92(6):063525, 2015. doi: 10.1103/PhysRevD.92.063525.

C. S. Alves et al. Mon. Not. R. Astron. Soc., 488(3):3607–3624, 07 2019.

L. Amendola, M. Kunz, and D. Sapone. JCAP, 04:013, 2008. doi: 10.1088/1475-7516/2008/04/013.

J. Asorey&Hale et al. In Advancing Astrophysics with the SKA – II (AASKAII). 2026. arXiv search: Report number AASKAII/Asorey01.

V. Assassi, M. Simonović, and M. Zaldarriaga. JCAP, 11:054, 2017. doi: 10.1088/1475-7516/2017/11/054.

P. Auclair et al. Living Rev. Rel., 26(1):5, 2023. doi: 10.1007/s41114-023-00045-2.

E. Babichev and C. Deffayet. Class. Quant. Grav., 30:184001, 2013. doi: 10.1088/0264-9381/30/18/184001.

D. J. Bacon et al. Mon. Not. R. Astron. Soc., 443(3):1900–1915, Sept. 2014. doi: 10.1093/mnras/stu1270.

T. Baker et al. Rev. Mod. Phys., 93(1):015003, 2021. doi: 10.1103/RevModPhys.93.015003.

R. Barkana. Nature, 555(7694):71–74, 2018. doi: 10.1038/nature25791.

J. Beltrán Jiménez, L. Heisenberg, and T. S. Koivisto. Universe, 5(7):173, 2019. doi: 10.3390/universe5070173.

F. Bernardeau, C. Bonvin, and F. Vernizzi. Phys. Rev. D, 81(8):083002, Apr. 2010. doi: 10.1103/PhysRevD.81.083002.

G. Bernstein and B. Jain. Astrophys. J., 600(1):17–25, Jan. 2004. doi: 10.1086/379768.

M. Berti et al. JCAP, 01(01):018, 2022. doi: 10.1088/1475-7516/2022/01/018.

F. Beutler and E. Di Dio. J. Cosmol. Astropart. Phys., 2020(7):048, July 2020. doi: 10.1088/1475-7516/2020/07/048.

S. Bharadwaj, B. B. Nath, and S. K. Sethi. Journal of Astrophysics and Astronomy, 22(1):21–34, Mar. 2001. doi: 10.1007/BF02933588.

C. Bonvin and R. Durrer. Phys. Rev. D, 84:063505, 2011. doi: 10.1103/PhysRevD.84.063505.

C. Bonvin and P. Fleury. JCAP, 05:061, 2018. doi: 10.1088/1475-7516/2018/05/061.

C. Bonvin and L. E. Pogosian. Nature Astron., 7(9):1023–1024, 2023. doi: 10.1038/s41550-023-02026-5.

C. Bonvin, L. Hui, and E. Gaztanaga. Phys. Rev. D, 89(8):083535, 2014. doi: 10.1103/PhysRevD.89.083535.

M. Bruni et al. Phys. Rev. D, 85:041301, 2012. doi: 10.1103/PhysRevD.85.041301.

S. Camera, R. Maartens, and M. G. Santos. Mon. Not. R. Astron. Soc., 451:L80–L84, July 2015. doi: 10.1093/mnrasl/slv069.

S. Camera et al. PoS, AASKA14:025, 2015. doi: 10.22323/1.215.0025.

S. Casas et al. Phys. Dark Univ., 39:101151, 2023. doi: 10.1016/j.dark.2022.101151.

S. Castello. A Matter of Time: Testing Gravity and Dark Matter with the Distortion of Time in Galaxy Surveys. PhD thesis, University of Geneva, 2025.

S. Castello, N. Grimm, and C. Bonvin. Phys. Rev. D, 106(8):083511, 2022. doi: 10.1103/PhysRevD.

106.083511.
S. Castello et al. JCAP, 05:003, 2024a. doi: 10.1088/1475-7516/2024/05/003.
S. Castello et al. Phys. Rev. D, 110(10):103523, 2024b. doi: 10.1103/PhysRevD.110.103523.
S. Castello, Z. Zheng, C. Bonvin, and L. Amendola. Phys. Rev. D, 111(12):123559, 2025. doi: 10.1103/1my7-zklj.
E. Castorina and E. Di Dio. J. Cosmol. Astropart. Phys., 2022(1):061, Jan. 2022. doi: 10.1088/1475-7516/2022/01/061.
E. Castorina and M. White. Mon. Not. R. Astron. Soc., Feb. 2018. ISSN 1365-2966. doi: 10.1093/mnras/sty410. URL http://dx.doi.org/10.1093/mnras/sty410.
P. G. Castro, A. F. Heavens, and T. D. Kitching. Phys. Rev. D, 72(2):023516, July 2005. doi: 10.1103/PhysRevD.72.023516.
A. Challinor and A. Lewis. Phys. Rev. D, 84:043516, 2011. doi: 10.1103/PhysRevD.84.043516.
C. Clarkson et al. Mon. Not. Roy. Astron. Soc., 486(1):L101–L104, 2019. doi: 10.1093/mnrasl/slz066.
T. Clifton, P. G. Ferreira, A. Padilla, and C. Skordis. Phys. Rep., 513(1):1–189, Mar. 2012. doi: 10.1016/j.physrep.2012.01.001.
S. Cunnington, S. Camera, and A. Pourtsidou. Mon. Not. R. Astron. Soc., 499(3):4054–4067, Dec. 2020. doi: 10.1093/mnras/staa2986.
S. Cunnington et al. Mon. Not. R. Astron. Soc., 523(2):2453–2477, Aug. 2023. doi: 10.1093/mnras/stad1567.
C. Deffayet, X. Gao, D. A. Steer, and G. Zahariade. Phys. Rev. D, 84:064039, 2011. doi: 10.1103/PhysRevD.84.064039.
DES Collaboration: Abbott et al. arXiv e-prints, art. arXiv:2503.13632, Mar. 2025. doi: 10.48550/arXiv.2503.13632.
DESI Collaboration: Abareshi et al. Astron. J., 164(5):207, Nov. 2022. doi: 10.3847/1538-3881/ac882b.
DESI Collaboration: Abdul-Karim et al. arXiv e-prints, art. arXiv:2503.14745, Mar. 2025. doi: 10.48550/arXiv.2503.14745.
DESI Collaboration: Adame et al. J. Cosmol. Astropart. Phys., 9:008, Sept. 2025. doi: 10.1088/1475-7516/2025/09/008.
E. Di Dio, R. Durrer, G. Marozzi, and F. Montanari. JCAP, 12:017, 2014. doi: 10.1088/1475-7516/2014/12/017. [Erratum: JCAP 06, E01 (2015)].
E. Di Dio, R. Durrer, G. Marozzi, and F. Montanari. JCAP, 01:016, 2016. doi: 10.1088/1475-7516/2016/01/016.
E. Di Dio et al. JCAP, 03:006, 2017. doi: 10.1088/1475-7516/2017/03/006.
E. Di Dio et al. JCAP, 04:053, 2019. doi: 10.1088/1475-7516/2019/04/053.
S. Dlamini, S. Jolicoeur, and R. Maartens. European Physical Journal C, 84(1):95, Jan. 2024. doi: 10.1140/epjc/s10052-024-12467-5.
A. Dvornik et al. Astron. Astrophys., 675:A189, July 2023. doi: 10.1051/0004-6361/202245158.
D. M. Eardley, D. L. Lee, and A. P. Lightman. Phys. Rev. D, 8:3308–3321, Nov 1973a. doi: 10.1103/PhysRevD.8.3308. URL https://link.aps.org/doi/10.1103/PhysRevD.8.3308.
D. M. Eardley et al. Phys. Rev. Lett., 30:884–886, Apr 1973b. doi: 10.1103/PhysRevLett.30.884. URL https://link.aps.org/doi/10.1103/PhysRevLett.30.884.

Euclid Collaboration: Mellier et al. Astron. Astrophys., 697:A1, May 2025. doi: 10.1051/0004-6361/202450810.

J. Fonseca and C. Clarkson. J. Cosmol. Astropart. Phys., 2021(12):003, Dec. 2021. doi: 10.1088/1475-7516/2021/12/003.

J. Fonseca, S. Camera, M. Santos, and R. Maartens. Astrophys. J. Lett., 812(2):L22, 2015. doi: 10.1088/2041-8205/812/2/L22.

J. Fonseca et al. In Advancing Astrophysics with the SKA – II (AASKAII). 2026. arXiv search: Report number AASKAII/Fonseca01.

N. Frusciante and L. Perenon. Phys. Rept., 857:1–63, 2020. doi: 10.1016/j.physrep.2020.02.004.

B. Ghosh, R. Durrer, and E. Sellentin. J. Cosmol. Astropart. Phys., 2018(6):008, June 2018. doi: 10.1088/1475-7516/2018/06/008.

J. Gleyzes, D. Langlois, M. Mancarella, and F. Vernizzi. JCAP, 08:054, 2015. doi: 10.1088/1475-7516/2015/08/054.

H. S. Grasshorn Gebhardt and O. Doré. Phys. Rev. D, 104(12):123548, Dec. 2021. doi: 10.1103/PhysRevD.104.123548.

A. Hall, C. Bonvin, and A. Challinor. Phys. Rev. D, 87(6):064026, Mar. 2013. doi: 10.1103/PhysRevD.87.064026.

I. Harrison et al. In Advancing Astrophysics with the SKA – II (AASKAII). 2026a. arXiv search: Report number AASKAII/Harrison01.

I. Harrison et al. In Advancing Astrophysics with the SKA – II (AASKAII). 2026b. arXiv search: Report number AASKAII/Harrison02.

S. F. Hassan and R. A. Rosen. Phys. Rev. Lett., 108:041101, 2012. doi: 10.1103/PhysRevLett.108.041101.

L. Heisenberg. JCAP, 05:015, 2014. doi: 10.1088/1475-7516/2014/05/015.

R. W. Hellings and G. S. Downs. Astrophys. J. Lett., 265:L39–L42, Feb. 1983. doi: 10.1086/183954.

C. Heneka and L. Amendola. J. Cosmol. Astropart. Phys., 2018(10):004, Oct. 2018. doi: 10.1088/1475-7516/2018/10/004.

G. W. Horndeski. Int. J. Theor. Phys., 10:363–384, 1974. doi: 10.1007/BF01807638.

W. Hu and B. Jain. Phys. Rev. D, 70(4):043009, Aug. 2004. doi: 10.1103/PhysRevD.70.043009.

Y.-H. Hyun, Y. Kim, and S. Lee. Phys. Rev. D, 99:124002, Jun 2019. doi: 10.1103/PhysRevD.99.124002. URL https://link.aps.org/doi/10.1103/PhysRevD.99.124002.

M. Ishak. Living Reviews in Relativity, 22(1):1, Dec. 2019. doi: 10.1007/s41114-018-0017-4.

Ž. Ivezić et al. Astrophys. J., 873(2):111, Mar. 2019. doi: 10.3847/1538-4357/ab042c.

T. Jacobson. PoS, QG-PH:020, 2007. doi: 10.22323/1.043.0020.

G. Jelic-Cizmek, F. Lepori, C. Bonvin, and R. Durrer. JCAP, 04:055, 2021. doi: 10.1088/1475-7516/2021/04/055.

D. Jeong and F. Schmidt. Phys. Rev. D, 102(2):023530, 2020. doi: 10.1103/PhysRevD.102.023530.

D. Jeong, F. Schmidt, and C. M. Hirata. Phys. Rev. D, 85(2):023504, Jan. 2012. doi: 10.1103/PhysRevD.85.023504.

S. Jolicoeur et al. J. Cosmol. Astropart. Phys., 2021(6):039, June 2021. doi: 10.1088/1475-7516/2021/06/039.

N. Kaiser. Mon. Not. Roy. Astron. Soc., 227:1–27, 1987. doi: 10.1093/mnras/227.1.1.

D. Karagiannis, R. Maartens, and L. F. Randrianjanahary. J. Cosmol. Astropart. Phys., 2022(11): 003, Nov. 2022. doi: 10.1088/1475-7516/2022/11/003.

J. Khoury and A. Weltman. Phys. Rev. Lett., 93:171104, 2004. doi: 10.1103/PhysRevLett.93.171104.

H.-R. Klöckner et al. PoS, AASKA14:027, 2015. doi: 10.22323/1.215.0027.

D. Langlois and K. Noui. JCAP, 02:034, 2016. doi: 10.1088/1475-7516/2016/02/034.

E. V. Linder. Phys. Rev. D, 72:043529, 2005. doi: 10.1103/PhysRevD.72.043529.

X.-W. Liu, C. Heneka, and L. Amendola. J. Cosmol. Astropart. Phys., 2020(5):038, May 2020. doi: 10.1088/1475-7516/2020/05/038.

A. Loeb and J. S. B. Wyithe. Phys. Rev. Lett., 100(16):161301, Apr. 2008. doi: 10.1103/PhysRevLett.100.161301.

R. Maartens, F. B. Abdalla, M. Jarvis, and M. G. Santos. PoS, AASKA14:016, 2015. doi: 10.22323/1.215.0016.

R. Maartens et al. JCAP, 04:013, 2021. doi: 10.1088/1475-7516/2021/04/013.

C. M. J. Marques, C. J. A. P. Martins, and C. S. Alves. FRIDDA: Fisher foRecast code for combIned reDshift Drift and Alpha. Astrophysics Source Code Library, record ascl:2305.001, May 2023.

P. McDonald. Journal of Cosmology and Astroparticle Physics, 2009(11):026–026, Nov. 2009. ISSN 1475-7516. doi: 10.1088/1475-7516/2009/11/026. URL http://dx.doi.org/10.1088/1475-7516/2009/11/026.

P. McDonald and U. Seljak. J. Cosmol. Astropart. Phys., 2009(10):007, Oct. 2009. doi: 10.1088/1475-7516/2009/10/007.

S. Minin and F. Kamalabadi. Appl. Opt., 48(36):6913, Dec. 2009. doi: 10.1364/AO.48.006913.

T. Montandon et al. JCAP, 08:043, 2023. doi: 10.1088/1475-7516/2023/08/043.

T. Montandon, E. Di Dio, C. Rampf, and J. Adamek. 1 2025.

F. Montano and S. Camera. Physics of the Dark Universe, 46:101570, Dec. 2024a. doi: 10.1016/j.dark.2024.101570.

F. Montano and S. Camera. Physics of the Dark Universe, 46:101634, Dec. 2024b. doi: 10.1016/j.dark.2024.101634.

A. Nasirudin et al. In Advancing Astrophysics with the SKA – II (AASKAII). 2026. arXiv search: Report number AASKAII/Nasirudin01.

S. Navas et al. Phys. Rev. D, 110(3):030001, 2024. doi: 10.1103/PhysRevD.110.030001.

M. Noorikuhani and R. Scoccimarro. Physical Review D, 107(8), Apr. 2023. ISSN 2470-0029. doi: 10.1103/physrevd.107.083528. URL http://dx.doi.org/10.1103/PhysRevD.107.083528.

R. P. Norris et al. Publ. Astron. Soc. Aust., 28(3):215–248, Aug. 2011. doi: 10.1071/AS11021.

M. Novara, F. Montano, and S. Camera. arXiv e-prints, art. arXiv:2509.08056, Sept. 2025. doi: 10.48550/arXiv.2509.08056.

D. Obreschkow et al. Astrophys. J., 703(2):1890–1903, Oct. 2009. doi: 10.1088/0004-637X/703/2/1890.

T. Padmanabhan. Phys. Rept., 380:235–320, 2003. doi: 10.1016/S0370-1573(03)00120-0.

P. Paul, C. Clarkson, and R. Maartens. JCAP, 04:067, 2023. doi: 10.1088/1475-7516/2023/04/067.

P. Paul, C. Clarkson, and R. Maartens. Phys. Rev. Lett., 133(12):121001, 2024. doi: 10.1103/PhysRevLett.133.121001.

P. J. Peebles. The Large-Scale Structure of the Universe. Princeton University Press, 11 1980. ISBN 978-0-691-08240-0, 978-0-691-20983-8, 978-0-691-20671-4.

B. B. P. Perera et al. Mon. Not. Roy. Astron. Soc., 490(4):4666–4687, 2019. doi: 10.1093/mnras/stz2857.

Planck Collaboration: Aghanim et al. Astron. Astrophys., 641:A6, 2020. doi: 10.1051/0004-6361/201833910. [Erratum: Astron.Astrophys. 652, C4 (2021)].

L. Pogosian, A. Silvestri, K. Koyama, and G.-B. Zhao. Phys. Rev. D, 81:104023, 2010. doi: 10.1103/PhysRevD.81.104023.

A. Pourtsidou, C. Skordis, and E. J. Copeland. Phys. Rev. D, 88(8):083505, 2013. doi: 10.1103/PhysRevD.88.083505.

A. Rassat and A. Refregier. Astron. Astrophys., 540:A115, Apr. 2012. doi: 10.1051/0004-6361/201118638.

P. Reimberg, F. Bernardeau, and C. Pitrou. J. Cosmol. Astropart. Phys., 2016(1):048–048, Jan. 2016. doi: 10.1088/1475-7516/2016/01/048.

B. A. R. Rocha and C. J. A. P. Martins. Mon. Not. R. Astron. Soc., 518(2):2853–2869, 11 2022.

S. Rossiter, S. Camera, C. Clarkson, and R. Maartens. arXiv e-prints, art. arXiv:2407.06301, July 2024. doi: 10.48550/arXiv.2407.06301.

S. J. Rossiter et al. arXiv e-prints, art. arXiv:2603.00244, Feb. 2026. doi: 10.48550/arXiv.2603.00244.

Z. Sakr. arXiv e-prints, art. arXiv:2601.16899, Jan. 2026. doi: 10.48550/arXiv.2601.16899.

A. Sandage. Astrophys. J., 136:319, Sept. 1962. doi: 10.1086/147385.

M. Santos et al. In MeerKAT Science: On the Pathway to the SKA, page 32, Jan. 2016. doi: 10.22323/1.277.0032.

C. S. Saraf et al. arXiv e-prints, art. arXiv:2505.05821, May 2025. doi: 10.48550/arXiv.2505.05821.

R. Scoccimarro. Phys. Rev. D, 92(8):083532, Oct. 2015. doi: 10.1103/PhysRevD.92.083532.

U. Seljak. Phys. Rev. Lett., 102:021302, 2009. doi: 10.1103/PhysRevLett.102.021302.

T. W. Shimwell et al. Astron. Astrophys., 598:A104, Feb. 2017. doi: 10.1051/0004-6361/201629313.

SKA Cosmology SWG: Bacon et al. Publ. Astron. Soc. Austral., 37:e007, 2020. doi: 10.1017/pasa.2019.51.

D. Sobral-Blanco and C. Bonvin. Phys. Rev. D, 104(6):063516, 2021. doi: 10.1103/PhysRevD.104.063516.

D. N. Spergel and P. J. Steinhardt. Phys. Rev. Lett., 84:3760–3763, 2000. doi: 10.1103/PhysRevLett.84.3760.

The LSST Dark Energy Science Collaboration: Mandelbaum et al. arXiv e-prints, art. arXiv:1809.01669, Sept. 2018. doi: 10.48550/arXiv.1809.01669.

S. Tulin and H.-B. Yu. Phys. Rept., 730:1–57, 2018. doi: 10.1016/j.physrep.2017.11.004.

I. Tutusaus, D. Sobral-Blanco, and C. Bonvin. Phys. Rev. D, 107(8):083526, 2023. doi: 10.1103/PhysRevD.107.083526.

O. Umeh, S. Jolicoeur, R. Maartens, and C. Clarkson. J. Cosmol. Astropart. Phys., 2017(3):034, Mar. 2017. doi: 10.1088/1475-7516/2017/03/034.

J. P. W. Verbiest, S. Osłowski, and S. Burke-Spolaor. Pulsar Timing Array Experiments, pages 1–42. Springer Singapore, Singapore, 2021. ISBN 978-981-15-4702-7. doi: 10.1007/

978-981-15-4702-7_4-1. URL https://doi.org/10.1007/978-981-15-4702-7_4-1.

J.-A. Viljoen, J. Fonseca, and R. Maartens. J. Cosmol. Astropart. Phys., 2020(9):054, Sept. 2020. doi: 10.1088/1475-7516/2020/09/054.

S. Weinberg. Rev. Mod. Phys., 61:1–23, 1989. doi: 10.1103/RevModPhys.61.1.

A. Weltman et al. Publ. Astron. Soc. Aust., 37:e002, Jan. 2020. doi: 10.1017/pasa.2019.42.

M. White, Y.-S. Song, and W. J. Percival. Mon. Not. R. Astron. Soc., 397(3):1348–1354, Aug. 2009. ISSN 1365-2966. doi: 10.1111/j.1365-2966.2008.14379.x. URL http://dx.doi.org/10.1111/j.1365-2966.2008.14379.x.

L. Wolz et al. In Advancing Astrophysics with the SKA – II (AASKAII). 2026. arXiv search: Report number AASKAII/Wolz01.

P.-J. Wu and X. Zhang. J. Cosmol. Astropart. Phys., 2022(1):060, Jan. 2022. doi: 10.1088/1475-7516/2022/01/060.

P.-J. Wu, Y. Li, J.-F. Zhang, and X. Zhang. Science China Physics, Mechanics, and Astronomy, 66 (7):270413, July 2023. doi: 10.1007/s11433-022-2104-7.

S. Yahya et al. Mon. Not. R. Astron. Soc., 450(3):2251–2260, 05 2015.

K. Yamamoto et al. Publ. Astron. Soc. Jpn, 58:93–102, Feb. 2006. doi: 10.1093/pasj/58.1.93.

J. Yoo and V. Desjacques. Phys. Rev. D, 88(2):023502, July 2013. doi: 10.1103/PhysRevD.88.023502.

J. Yoo, A. L. Fitzpatrick, and M. Zaldarriaga. Phys. Rev. D, 80:083514, 2009. doi: 10.1103/PhysRevD.80.083514.

S. Zaroubi and Y. Hoffman. arXiv e-prints, art. astro-ph/9311013, Nov. 1993. doi: 10.48550/arXiv.astro-ph/9311013.

P. Zhang, M. Liguori, R. Bean, and S. Dodelson. Phys. Rev. Lett., 99:141302, 2007. doi: 10.1103/PhysRevLett.99.141302.